Article

TRANSPARENT PROCESS

EMBO reports

Induction of hematopoietic and endothelial cell program orchestrated by ETS transcription factor ER71/ETV2

Fang Liu[1], Daofeng Li[2], Yik Yeung Lawrence Yu[1], Inyoung Kang[1], Min-Ji Cha[1,†], Ju Young Kim[3], Changwon Park[3], Dennis K Watson[4], Ting Wang[2,*] & Kyunghee Choi[1,5,**]

Abstract

The ETS factor ETV2 (aka ER71) is essential for the generation of the blood and vascular system, as ETV2 deficiency leads to a complete block in blood and endothelial cell formation and embryonic lethality in the mouse. However, the ETV2-mediated gene regulatory network and signaling governing hematopoietic and endothelial cell development are poorly understood. Here, we map ETV2 global binding sites and carry out *in vitro* differentiation of embryonic stem cells, and germ line and conditional knockout mouse studies to uncover mechanisms involved in the hemangiogenic fate commitment from mesoderm. We show that ETV2 binds to enhancers that specify hematopoietic and endothelial cell lineages. We find that the hemangiogenic progenitor population in the developing embryo can be identified as FLK1^{high}PDGFRα^{-}. Notably, these hemangiogenic progenitors are exclusively sensitive to ETV2-dependent FLK1 signaling. Importantly, ETV2 turns on other Ets genes, thereby establishing an ETS hierarchy. Consequently, the hematopoietic and endothelial cell program initiated by ETV2 is maintained partly by other ETS factors through an ETS switching mechanism. These findings highlight the critical role that transient ETV2 expression plays in the regulation of hematopoietic and endothelial cell lineage specification and stability.

Keywords ChIP-Seq; ER71/ETV2; ETS hierarchy; ETS switching; hemangioblast; VEGFR2/FLK1

Subject Categories Development & Differentiation; Transcription; Chromatin, Epigenetics, Genomics & Functional Genomics

DOI 10.15252/embr.201439939 | Received 2 December 2014 | Revised 24 February 2015 | Accepted 26 February 2015 | Published online 23 March 2015

EMBO Reports (2015) 16: 654–669

Introduction

Functional blood and its conduit vascular system are the first to form during embryogenesis. Blood cells in the developing embryo are generated in close association with endothelial cells. For example, yolk sac blood islands composed of centrally located embryonic blood cells and an outer luminal layer of endothelial cells of the embryo are generated from the extra-embryonic mesoderm presumably through a hemangioblast intermediary [1–4]. While the hemangioblast is believed to be a common hematopoietic and endothelial cell progenitor, a recent study suggests that primitive erythroid cells in the yolk sac are developmentally distinct from the yolk sac endothelium [5]. It has also been suggested that hemangioblast is not a progenitor, but represents a competent cell state that can generate either blood or endothelium depending on the surrounding signals [6]. Regardless, it is now widely accepted that hemogenic endothelium within the dorsal aorta of the embryo is the cell origin of the definitive hematopoietic system [7–10]. Later in adult life, hematopoietic system is maintained partly through the vascular system. As such, sinusoidal endothelial cells form an important component of the niche in which hematopoietic stem cells reside [11–13]. It is thus noticeable that many transcription factors and signaling pathways are largely shared between blood and endothelial cells. Gene-targeting studies have shown that mutations in any of the shared genes often affect both cell lineages, supporting the notion of common genetic pathways regulating hematopoietic and endothelial cell lineage development and function. Remarkably, *Vegfa*- or *Vegfr2* (*Flk1*)-deficient animals completely fail to generate blood and blood vessels and die early in embryogenesis, indicating that precise VEGFA signaling via FLK1 is critical for the proper formation of the blood and vascular systems [14–16]. Clearly, molecular mechanisms by which blood and vessel lineages are specified in the developing embryo need to be better elucidated. Such information in turn would be greatly useful for future applications for blood and

1 Department of Pathology and Immunology, Washington University School of Medicine, St. Louis, MO, USA
2 Department of Genetics, Center for Genome Sciences and Systems Biology, Washington University School of Medicine, St. Louis, MO, USA
3 Department of Pediatrics, Children's Heart Research and Outcomes Center, Emory University School of Medicine, Atlanta, GA, USA
4 Department of Pathology and Laboratory Medicine, Medical University of South Carolina, Charleston, SC, USA
5 Developmental, Regenerative, and Stem Cell Biology Program, Washington University School of Medicine, St. Louis, MO, USA
*Corresponding author. Tel: +1 3142 860865; E-mail: twang@genetics.wustl.edu
**Corresponding author. Tel: +1 3143 628716; E-mail: kchoi@wustl.edu
†Present address: Catholic Kwandong University, Institute for Bio-Medical Convergence, College of Medicine, Korea

© 2015 The Authors

vascular repair and regeneration as well as for obtaining hematopoietic and endothelial cells from pluripotent stem cells.

ETS transcription factors have emerged as critical regulators of hematopoietic and vascular development [17–19]. The ETS domain, which is composed of a winged helix-turn-helix motif, binds a consensus sequence (GGAA/T) to regulate target gene expression. Many ETS factors are redundantly expressed in blood and endothelial cells. Consistently, mice or zebrafish deficient in *Ets* factors display differing levels of hematopoietic and vascular defects [20–23]. Distinct from other ETS factors, *Etv2* is transiently expressed in the primitive streak, yolk sac blood islands, and large vessels including the dorsal aorta during embryogenesis [24]. Remarkably, *Etv2*-deficient animals display a complete block in blood and blood vessel formation, indicating that ETV2 performs a non-redundant and indispensable function in hematopoietic and vessel development [24–27]. As such, *Etv2* inactivation leads to similar hematopoietic and vascular defects to those of *Vegfa* or *Flk1* deficiency. Herein, we characterized germ line and conditional *Etv2* knockout mice and performed genomewide ChIP-Seq of ETV2 using *in vitro* differentiated embryonic stem (ES) cells to better understand how ETV2 can achieve such a non-redundant predominant role in hematopoietic and endothelial cell development. We discover that specification of the hemangiogenic program requires ETV2 activation of the blood and endothelial cell lineage-specifying genes and VEGF signaling. Moreover, ETV2 establishes an ETS hierarchy by directly activating other *Ets* genes, which then maintain blood and endothelial cell program initiated by ETV2 through an ETS switching mechanism. Collectively, we provide molecular and cellular basis by which ETV2 establishes the hematopoietic and endothelial cell program.

Results

ETV2 ChIP-Seq and target gene identification

To understand ETV2-mediated genetic program regulating hematopoietic and endothelial cell lineage development, we performed ETV2 ChIP-Seq analysis using *in vitro* differentiated embryonic stem (ES) cells. We previously described A2 ES cells expressing ETV2-V5 in a doxycycline (DOX)-inducible manner [24,27]. DOX addition from day 2 to 3.5, a time frame when *Etv2* is normally expressed, in these cells robustly induced hemangioblast formation. To facilitate ETV2 target identification, we additionally generated polyclonal antibodies against $ETV2_{200–219}$ peptide (ETV2-polyAbs) to pull down ETV2-associated chromatin. Two independent biological replicates from DOX-treated day 3.5 *iEtv2* EB cells were subjected to ETV2-polyAbs and V5 ChIP and deep sequencing using IgG as controls. Sequencing reads were mapped to the mouse genome assembly mm9 provided by the UCSC Genome Browser [28]. Using MACS2 [29] at a *P*-value cutoff of 1E-6, we identified 8,019 ETV2 binding peaks from the ETV2-polyAbs samples and 11,892 ETV2 binding peaks from the V5 samples (Supplementary Table S1). We focused our analysis on the 3,933 peaks that overlapped between the ETV2-polyAbs samples and the V5 samples (Fig 1A and B), as we reasoned that this strategy provided the best balance between sensitivity and specificity given the genomic technology we employed. As such, the ETV2 overexpression system ensures higher sensitivity of detection of ETV2 genomewide target sites than assaying against endogenous protein. Moreover, focusing on reproducible ChIP-seq peaks based on independent antibodies ensures a higher specificity. Indeed, several initial quality assurance analyses suggested that these ETV2 binding peaks had high quality and were connected to ETV2 biology, supporting that they were bona fide biological target sites of ETV2. First, raw read densities within these ETV2 peaks were highly reproducible between experiments (cc = 0.974 for ETV2-polyAbs and 0.969 for V5 between replicates, cc = 0.993 between the two antibodies, Supplementary Fig S1A–C). ChIP-Seq signals were highly enriched in peak centers across samples when compared to surrounding genomic regions or control (Fig 1A and B). We also identified the most significant sequence motif associated with the ChIP-Seq peaks (Fig 1C). This motif, which represented ~85% of the peaks, matched perfectly with the known binding specificity of other ETS factors, FLI1, and ERG [30]. We additionally identified GATA, SOX, or E-box motifs to be frequently associated with the ETV2 peaks (Supplementary Fig S1D). Genomewide distribution of these binding peaks was far from random expectation, with ~14% significant enrichment in the promoter regions and ~70% in introns or intergenic regions, suggesting that ETV2 functions by interacting with both gene promoters and distal enhancers (Fig 1D and Supplementary Fig S1F). We next subjected these ETV2 binding peaks to a GREAT analysis [31] to understand the overall ETV2-mediated biological function and found that they were strongly associated with endothelial and hematopoietic cell lineage development and differentiation (Fig 1E, for complete result see Supplementary Table S2A). Finally, we examined evolutionary conservation of sequences associated with ETV2 peaks and found that they are much more conserved than their neighboring sequences (Fig 1F). Indeed, 2,231 (56.7%) peaks overlapped with conserved elements determined based on 30-way vertebrate alignment [32] from the UCSC Genome Browser (P-value < $2.2e^{-16}$, binomial test), suggesting that the identified peaks were strongly enriched for functionally constrained sequences. As the majority of the ETV2 binding peaks were outside gene promoters, we reasoned that some of them could serve as distal enhancers. Connecting enhancers to their target genes is an extremely challenging problem, because enhancers do not necessarily regulate the nearest genes, nor do they necessarily regulate one single target genes. Therefore, we combined GREAT analysis with gene expression analysis to optimize sensitivity and specificity. Using GREAT default parameters, we defined a "basal regulatory domain" for each gene (Methods), and we associated an ETV2 ChIP-seq peak with a target gene if the peak was within the basal regulatory domain of the gene. This approach resulted in 4,580 ETV2 peak-associated genes.

To narrow down to a more confident list of direct target genes of ETV2, we integrated our ChIP-Seq data with gene expression pattern of $FLK1^+$ mesoderm isolated from control and iETV2 EB cells that were generated with DOX (from day 2–3.5) as well as $FLK1^+$ mesoderm sorted from $Etv2^{+/+}$ and $Etv2^{-/-}$ day 3.5 EBs [27]. ETV2 peak-associated genes were significantly enriched for genes that exhibited increased expression in the ETV2 overexpression system and/or reduced expression in the ETV2 knockout system (Fig 2A, P-value < 2.2E-16, hypergeometric test). On the other hand, there was no significant enrichment of genes with the opposite expression pattern (i.e., upregulated in ETV2 knockout and downregulated in ETV2 overexpression, Supplementary Fig S2A). This expression pattern suggested that ETV2 primarily functions as a transcriptional

© 2015 The Authors

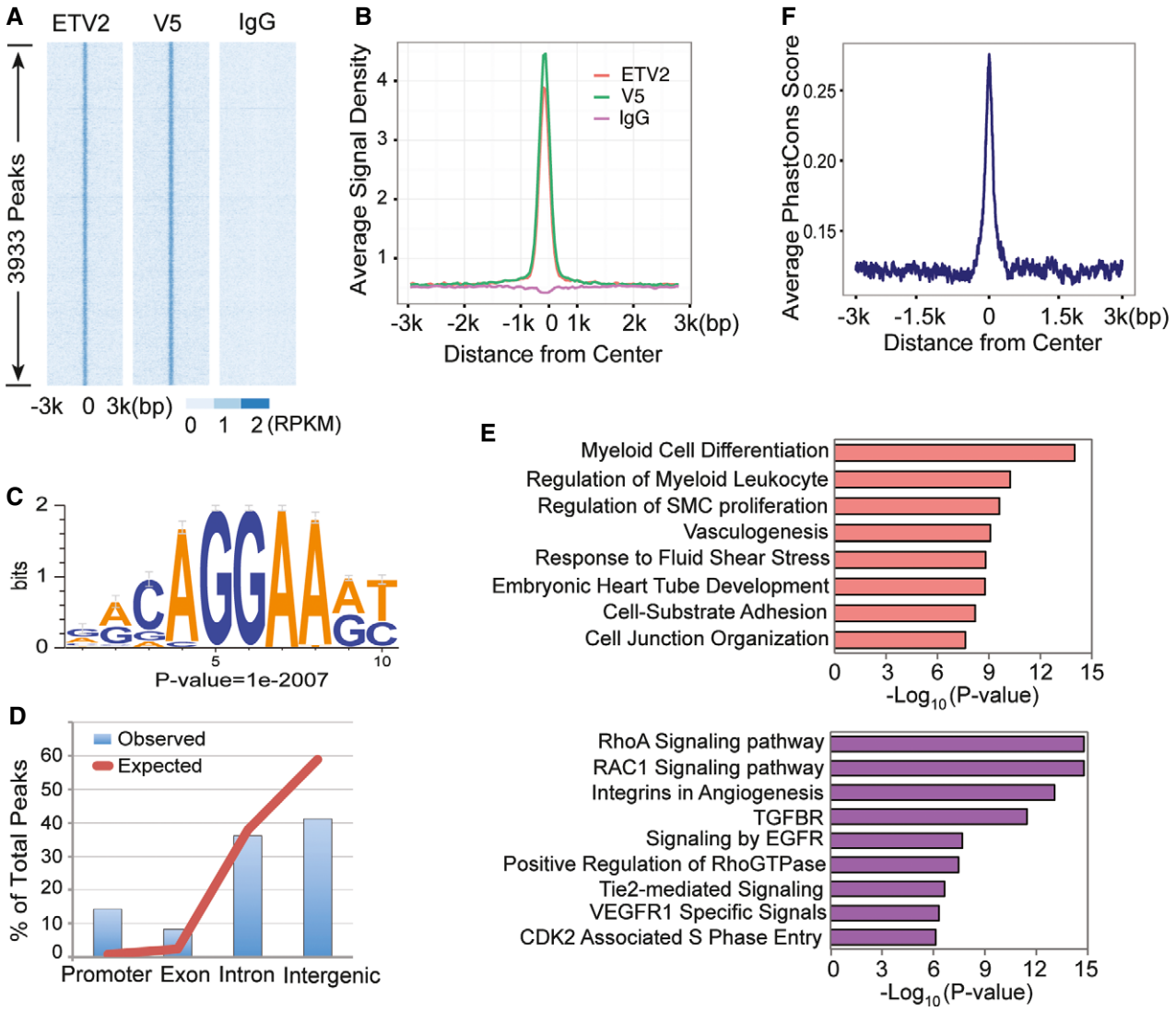

Figure 1. ChIP-Seq analysis of ETV2 binding regions.

A Heatmap of read density from each replicate in a 6-kb region flanking the peak centers.
B Averaged read density profile of each replicate in a 6-kb region flanking the peak center.
C ETV2 motif logo, *de novo* trained by Homer software using ChIP-Seq peaks.
D Distribution of ETV2 ChIP-Seq peaks in different genomic features. Red line represents genomic background (expectation), and blue bar represents observed peak distribution.
E Functional enrichment analysis of ChIP-Seq peaks.
F Conservation score (phastCon) in a 6-kb region flanking peak centers of all peaks.

activator. We identified 425 ETV2 peak-associated genes that exhibiting the expected expression difference. They constitute a group of high confidence, direct target genes of ETV2. Functional enrichment analysis revealed that this group of genes was considerably enriched for hematopoietic and endothelial cell lineage development and differentiation, with the enrichment level markedly improved from genes identified by ChIP-seq peaks alone (Supplementary Table S2B). Many genes that exhibited expression changes upon either ETV2 overexpression or ETV2 knockout did not associate with ETV2 binding peaks. They are potentially downstream but not direct targets of ETV2. Additionally, many ETV2 peak-associated genes did not show expression change, even though as a group they are strongly enriched for endothelial and hematopoietic cell relevant functions. These binding peaks could potentially be false positives, but could also reveal functions of ETV2 other than directly activating target genes. One such potential function could be to modulate chromatin structure to a permissive state that allows genes to express at future developmental stages. We thus examined the epigenetic landscape of ETV2 binding sites across several cell and tissue types. We took advantage of publicly available whole-genome bisulfite sequencing data of mouse embryonic stem cells, neural progenitor cells, as well as adult tissues [33,34] to examine epigenetic changes co-occurring with ETV2 binding, focusing on distal sites that potentially function as lineage-specific enhancers.

 © 2015 The Authors

Intriguingly, these ETV2 binding sites were largely methylated in ES cells. The relatively high DNA methylation levels were maintained in neuronal progenitor cells and cerebellum, but reduced in heart and bone marrow (Fig 2B and Supplementary Fig S2B).

ETV2 induces hematopoietic and endothelial cell lineage-specifying genes

ETV2 targets can be broadly categorized into hematopoietic and endothelial cell lineage-specifying genes, VEGF, Notch, Rho-GTPase, and MAP kinase pathway and *Ets* factors (Fig 2C). Specifically, *Flk1*, *Fli1*, *Erg*, *Gata2*, *Scl*, *Meis1*, *Lmo2*, *Tie2*, *VE-cadherin*, *Dll4*, and *Notch* were among the 425 genes, which play critical roles in hematopoietic and endothelial cell development (Figs 2C and D, 3A and 5A). While some of these peaks occur on previously identified regulatory regions, such as *VE-cadherin* [27], currently identified ChIP-Seq peaks represented unique peaks that have not been reported yet. We additionally compared transcriptional profiling among FLK1$^+$ cells generated by enforced *Etv2* expression, *Etv2*-deficient FLK1$^+$ cells [27], and genes immediately upregulated by *Etv2* expression [35]. There was a significant enrichment in genes involved in the VEGF and Notch signaling pathways, suggesting the

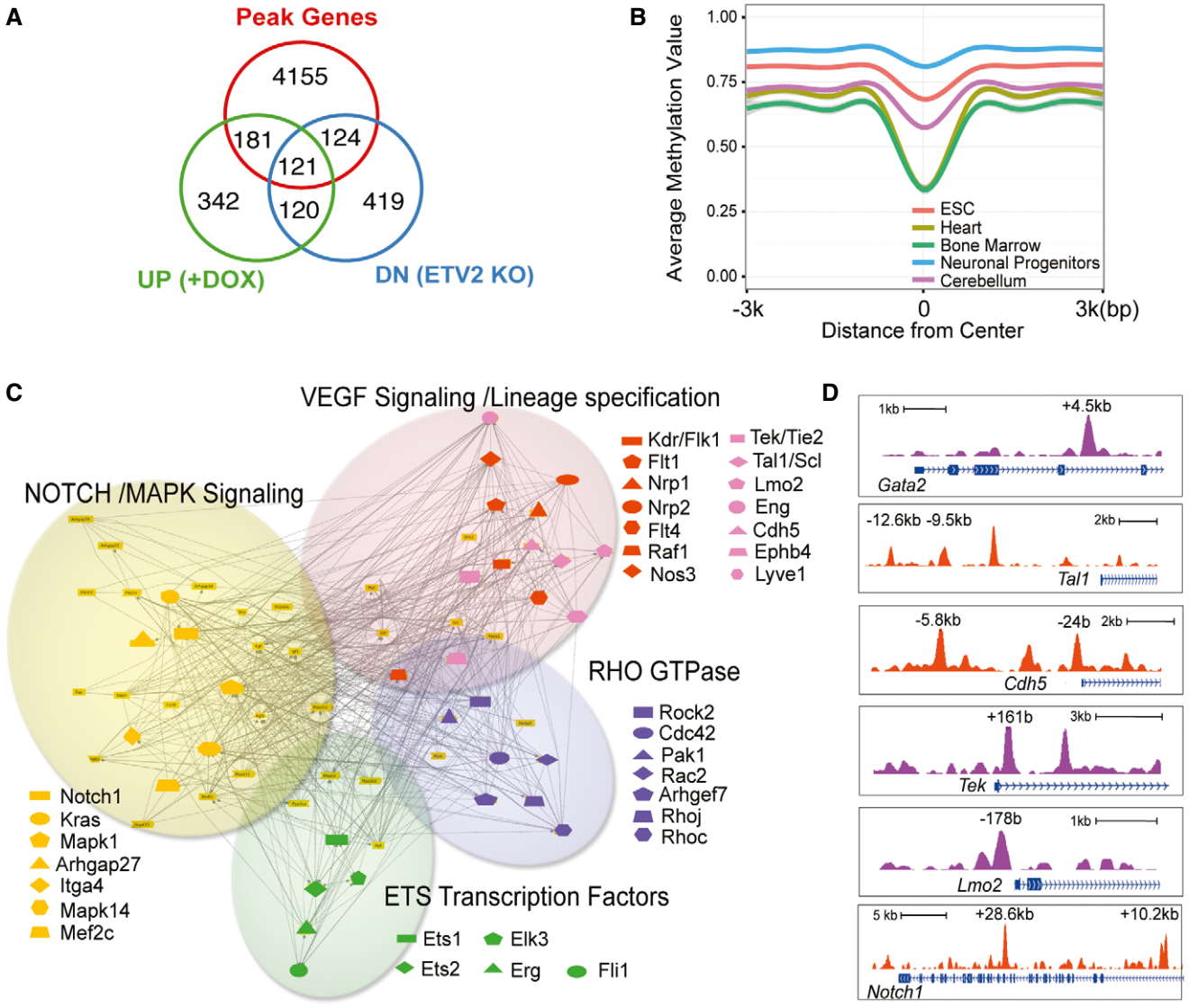

Figure 2. Identification of ETV2 downstream target genes and regulatory network.

A Venn diagram showing the overlap between ChIP-Seq peak-associated genes and ETV2 target genes identified by microarray data analysis. UP (+DOX): upregulated genes by ETV2 overexpression; DN (ETV2 KO): downregulated genes in ETV2 knockout.

B DNA methylation profile of ETV2 distal binding peaks. Averaged DNA methylation level was calculated using publicly available whole-genome bisulfite sequencing data from multiple cell and tissue types and plotted for a 6-kb region flanking peak centers.

C ETV2 gene regulatory network showing Notch/MAPK signaling, VEGF signaling/lineage specification, Rho-GTPase, and ETS transcription factor as downstream targets.

D Genomic snapshots depicting the ETV2 binding regions at the indicated genomic loci.

© 2015 The Authors

involvement of these pathways in hemangiogenic lineage development (Supplementary Fig S2C).

Previous studies have implicated the core gene regulatory network played by the ETS, GATA, and E-box motifs in hematopoietic and endothelial cell development [36]. *Etv2*, *Gata2,* and *Scl* can independently modulate hemangioblast development [37–39]. Moreover, coexpression of *Etv2*, *Gata2,* and *Scl* during the time of hemangioblast formation stage can robustly induce hemangioblast cell population [39]. Notably, GATA and E-box motifs were frequently associated with ETV2 peaks (Supplementary Fig S1D and E). Thus, we determined whether sequences representing binding sites of these factors occur in ETV2 peaks. We utilized the ChIP-Seq data of GATA2 and SCL from Wilson *et al* [30], which allowed us to train a positional weight matrix for each of these factors. GATA2 and SCL motifs were significantly enriched within the 3,933 peaks: 2,945, 609, and 484 co-occurrences of ETV2-SCL motifs (8-fold enrichment over random expectation, $P = 0$ from binomial test), ETV2-GATA2 motifs (14-fold enrichment, $P < 1.11E\text{-}35$), and ETV2-SCL-GATA2 motifs (15-fold enrichment, $P = 0$) (Supplementary Fig S2D). This observation is highly non-random, suggesting that ETV2 and these factors may interact or cobind to some of these sites. Indeed, ETV2 and GATA2 have been recently reported to form a complex to regulate hematopoietic and endothelial cell gene expression [40]. ETV2 presumably specifies the hemangiogenic cell fate by collectively turning on hematopoietic and endothelial cell lineage-specifying genes. The ETS, GATA, and E-box gene regulatory network is integral to this process.

ETV2 enhances VEGF signaling

ChIP-Seq analysis revealed ETV2 binding to VEGF receptors and downstream signaling pathway genes including MAPK. Specifically, ETV2 targets include *Flk1*, *Flt1*, *Flt4, Nrp1, Nrp2,* and *Mapk3* genes (Fig 3A). Rho-GTPases and adhesion molecules were also identified as potential ETV2 direct targets. We selected 15 peak regions associated with *Flk1*, *Flt1*, *Nrp1,* and *Nrp2* genes occupied by ETV2, of which 14 were evolutionarily conserved (Fig 3A and Supplementary Table S3), and validated ETV2 binding in day 3.5 *iEtv2* EBs using ChIP-qPCR. A significant mean enrichment was observed for ETV2 binding at these genomic locations with chromatin pulled down by V5 antibody or endogenous ETV2 antibody (ETV2-polyAbs) in *iEtv2* EB cells (Dox added on day 2) (Fig 3B). Importantly, ETV2 binding at these genomic locations was confirmed in R1 wild-type EB cells using ETV2-polyAbs, validating that these are *bona fide* ETV2 targets (Supplementary Fig S3A). To assess the functional significance of the ETV2 binding, we tested these regions for the response to ETV2 using the luciferase reporter assay. We found that ETV2 could activate the luciferase constructs tested, approximately 5- to 100-folds, compared to the pGL4 vector control (Fig 3C). We further selectively deleted the ETV2 binding motif in several reporter vectors and found that the luciferase activity was greatly impaired when ETV2 binding motif was deleted (Fig 3C). Collectively, these regions may act as ETV2 *cis*-regulatory elements for VEGF receptor gene expression. Future *in vivo* transgenic reporter system would further solidify such notion.

As ChIP-Seq analysis suggested that ETV2 could elevate FLK1 signaling activity, we determined whether ETV2 could directly modulate VEGF signaling. To this end, we performed VEGF signaling and Cell Motility PCR array, which included Rho-GTPases, adhesion and integrin genes, using RNA obtained from *iEtv2* EBs (differentiated ES cells) with DOX [27]. Strikingly, VEGF signaling pathway genes were upregulated by *Etv2* overexpression, which were reciprocally downregulated in $Etv2^{-/-}$ embryos as well as $Flk1^{-/-}$ embryos (Fig 3D and E, Supplementary Table S4). Additionally, while Rho-GTPase and its activating protein genes were upregulated by *Etv2* overexpression, they were greatly downregulated in E8.5 $Flk1^{-/-}$ embryos [41] (Fig 3F and G, Supplementary Table S5). These studies support the notion that hemangiogenic program specification requires ETV2-mediated FLK1 signaling activation.

ETV2 is required for the formation and expansion of FLK1$^+$ hemangiogenic progenitors

Consistent with the data that ETV2 enhances VEGF signaling, previous findings suggested that blood and endothelial cell progenitors express high levels of FLK1 (FLK1^{high}) compared to other FLK1-expressing cardiac or muscle progenitors (FLK1^{low}) [42]. To determine whether we can identify differential FLK1 activity associated with hemangiogenic cell population development in the embryo, we subjected embryos to FLK1 and PDGFRα expression analysis. As FLK1$^+$PDGFRα$^-$ cells isolated from differentiating ES cells were enriched for the hemangioblast [27] and as FLK1$^+$PDGFRα$^-$ cells in the developing embryo have not been characterized yet, we initially analyzed FLK1 and PDGFRα expression kinetics in developing embryos. In wild-type embryos, FLK1$^+$PDGFRα$^-$ hemangiogenic progenitors were already detected around embryonic day (E) 7.5 and progressively expanded with time during the course of E7.5–E8.5 (Fig 4A). Notably, the mean fluorescence intensity of the FLK1 staining within the FLK1$^+$PDGFRα$^-$ cell population became greater as embryos develop, suggesting an elevated FLK1 signaling activity within FLK1$^+$PDGFRα$^-$ cells compared to FLK1$^+$PDGFRα$^+$ cells (Fig 4A). Remarkably, FLK1^{high}PDGFRα$^-$ cell population was exclusively missing in $Etv2^{-/-}$ embryos, indicating that ETV2 was specifically required for the stage of FLK1^{high}PDGFRα$^-$ cell generation in the embryo (Fig 4A, Supplementary Fig S3B and C).

Etv2 is transiently expressed in developing embryos and ES/EBs [24]. To determine whether *Etv2* was still required once FLK1$^+$ hemangioblast was formed, we conditionally deleted *Etv2* within *Flk1*-expressing cells, *Flk1Cre;Etv2* CKO, by crossing $Flk1^{+/Cre}$;$Etv2^{+/-}$ (or $Flk1^{+/Cre}$;$Etv2^{f/+}$) and $Etv2^{f/f}$ mice to generate $Flk1^{+/Cre}$;$Etv2^{f/-}$ (or $Flk1^{+/Cre}$;$Etv2^{f/f}$) mice. No live *Flk1Cre;Etv2* CKO mice were obtained at weaning. Timed matings between $Flk1^{+/Cre}$;$Etv2^{+/-}$ (or $Flk1^{+/Cre}$;$Etv2^{f/+}$) and $Etv2^{flf}$ mice were performed, and embryos were analyzed at different time points. *Flk1Cre;Etv2* CKO embryos died around E10.5, later than $Etv2^{-/-}$ mice that die around E9.5, and exhibited wrinkled yolk sacs with dispersed blood (Fig 4B). At E8.5, FLK1$^+$PDGFRα$^-$ cells were detected but at much reduced levels within E8.5 *Flk1Cre;Etv2* CKO embryos (Fig 4C, Supplementary Fig S3D). Consequently, the embryo proper of the mutants was relatively pale and small and showed fluid and blood accumulation in the pericardial cavities. Whole-mount PECAM1/CD31 staining revealed disorganized vasculatures in the mutants (Fig 4D). E8.5 mutant yolk sacs contained fewer hematopoietic progenitor cells (Fig 4E). CD31-expressing cells also appeared to be reduced in E9.5 yolk sacs (Supplementary Fig S3E). Consistent with the phenotypic defects, expression of hematopoietic and endothelial genes in *Flk1Cre;Etv2* CKO yolk sacs was also greatly reduced (Fig 4F

 © 2015 The Authors

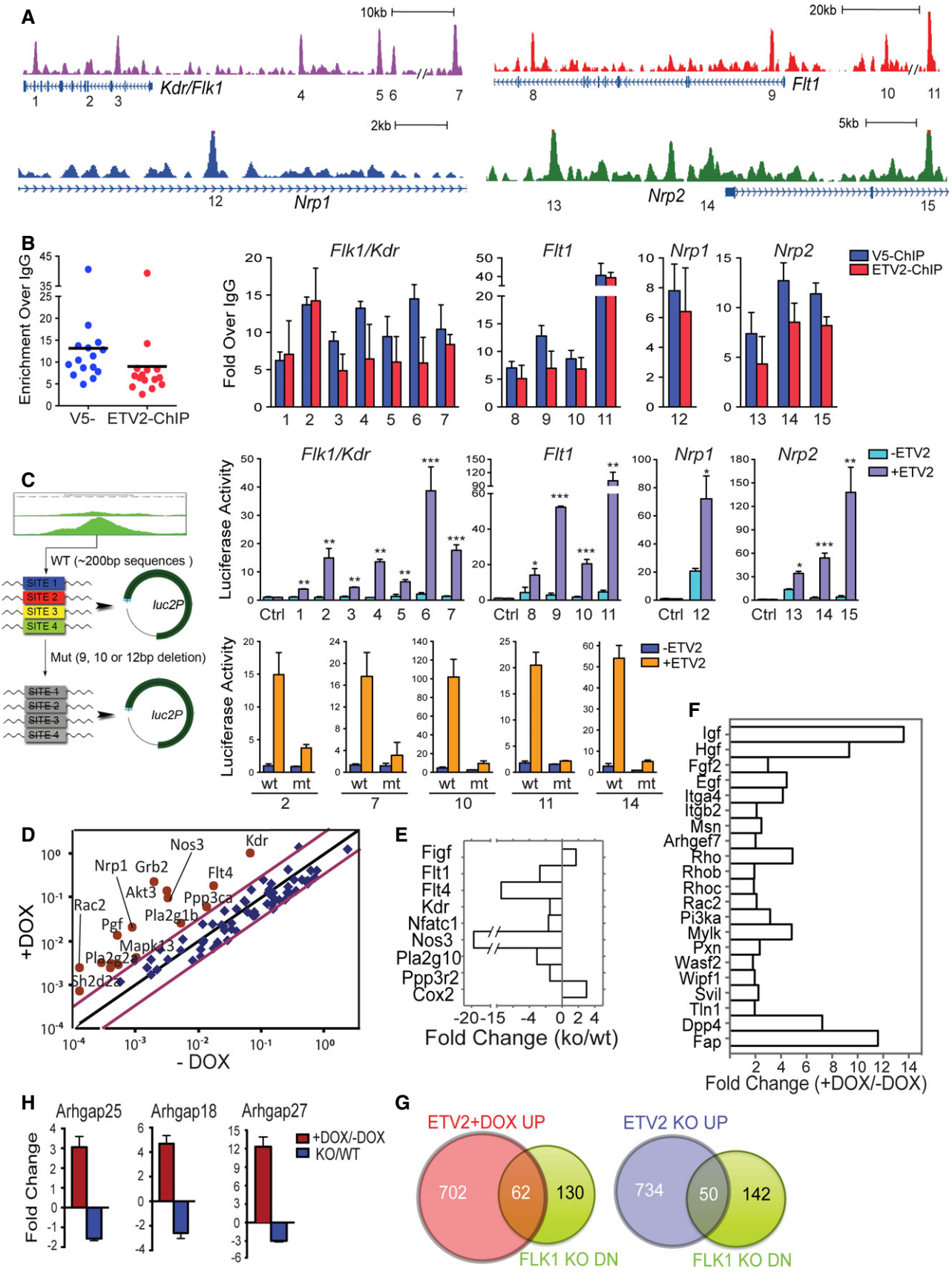
A
10kb
Kdr/Flk1
1 2 3 4 5 6 7
20kb
Flt1
8 9 10 11
2kb
Nrp1
12
5kb
Nrp2
13 14 15
B
Enrichment Over IgG
V5- ETV2-ChIP
Fold Over IgG
Flk1/Kdr
Flt1
Nrp1
Nrp2
V5-ChIP
ETV2-ChIP
C
WT (~200bp sequences)
SITE 1
SITE 2
SITE 3
SITE 4
luc2P
Mut (9, 10 or 12bp deletion)
Luciferase Activity
-ETV2
+ETV2
Ctrl
wt mt
D
+DOX
- DOX
Nos3
Kdr
Nrp1
Grb2
Flt4
Akt3
Ppp3ca
Rac2
Pla2g1b
Pgf
Mapk13
Pla2g2a
Sh2d2a
E
Figf
Flt1
Flt4
Kdr
Nfatc1
Nos3
Pla2g10
Ppp3r2
Cox2
Fold Change (ko/wt)
F
Igf
Hgf
Fgf2
Egf
Itga4
Itgb2
Msn
Arhgef7
Rho
Rhob
Rhoc
Rac2
Pi3ka
Mylk
Pxn
Wasf2
Wipf1
Svil
Tln1
Dpp4
Fap
Fold Change (+DOX/-DOX)
G
ETV2+DOX UP
702
62
130
FLK1 KO DN
ETV2 KO UP
734
50
142
FLK1 KO DN
H
Arhgap25
Arhgap18
Arhgap27
Fold Change
+DOX/-DOX
KO/WT

Figure 3.

Figure 3. ETV2 directly regulates VEGF receptors and activate VEGF signaling pathway.

A Genomic snapshots depicting the ETV2 binding peaks associated with the VEGFR genes. Numbers indicate ChIP-Seq peaks with high confidence.

B ChIP-PCR analysis showing ETV2 recruitment to the 15 potential binding sites in (A). ETV2 enrichments were shown by both V5 antibody and ETV2-polyAb pull-down. PCR primers and genomic locations are provided in Supplementary Table S3. Error bars represent SD, $n = 4$.

C Luciferase reporter assay for 1–15 ETV2 peak regions from (A). The indicated peak regions or selected ETV2 binding motif deletion mutants (2, 7, 10, 11, and 14) were cloned into the pGL4.24[*luc2P*/minP] vector (left panel). 293T cells were transfected with pGL4.24 control vector, ETV2 wild-type, or mutant luciferase reporter constructs, together with Renilla luciferase vector in the presence (pMSCV-*Etv2*) or absence of ETV2 expression plasmids. For each ETV2 peak reporter construct, luciferase activity was first normalized to Renilla luciferase values. Luciferase activity value obtained with ETV2 was then compared to that of the −ETV2 value. Error bars represent the SEM obtained from four biological replicates. *$P < 0.05$, **$P < 0.01$, ***$P < 0.001$, two-tailed Student's *t*-test.

D Mouse VEGF signaling array using RNA from day 3.5 *iEtv2* EBs (±DOX from day 2) is shown as scattered plots of fold changes (+DOX versus −DOX). Each gene was normalized to three housekeeping genes. Red dots are upregulated genes by DOX addition.

E RNA obtained from E8.5 $Etv2^{+/+}$ and $Etv2^{-/-}$ embryos was subjected to VEGF signaling analysis. Key genes with significant changes in expression are shown.

F Mouse Cell Motility PCR array using RNA from day 3.5 *iEtv2* EBs (±DOX from day 2) is shown as fold changes (+DOX versus −DOX).

G Venn diagram showing an overlap between downregulated genes in E8.5 $Flk1^{-/-}$ embryos [41] and upregulated genes by ETV2 overexpression (left) or ETV2 knockout (right) [27].

H Gene expression analysis of Rho-GTPase activating proteins 18, 25, and 27 in day 3 *iEtv2* (±DOX on day 2) or $Etv2^{+/+}$ and $Etv2^{-/-}$ EB cells. Genes were normalized to *Gapdh*. The fold change was obtained from the ratios of +DOX to −DOX or $Etv2^{-/-}$ to $Etv2^{+/+}$. Error bars represent the SD of four independent biological samples.

and G). Collectively, we conclude that ETV2 is required until sufficient $FLK1^{high}PDGFR\alpha^{-}$ cells are generated to guarantee proper blood and endothelial cell development.

ETS genes are ETV2 direct targets

Many ETS factors are potential ETV2 direct targets (Fig 5A and Supplementary Table S3). Importantly, *Etv2* was also identified as a target, suggesting that there is a positive auto-feedback regulation involving *Etv2* expression. We selected 15 peak regions associated with *Fli1, Ets1*, *Erg* and *Ets2* genes, of which 12 were conserved (Supplementary Table S3), and validated ETV2 binding on these genes (Fig 5B). We next constructed luciferase reporters using the validated peak regions of the *Ets* genes and found that all the tested fragments enhanced the luciferase activity by ETV2 (Fig 5C). Importantly, deletion of the respective ETV2 binding motifs resulted in substantially reduced luciferase activities (Fig 5D). In addition, we observed cooperative action among the potential ETV2 motifs. For example, while the deletion of the two binding sites (mt1) in the *Fli1* regulatory region (peak 7 in Fig 5A) still conferred the luciferase activity in response to ETV2, deletion of all three ETV2 binding motifs (mt2 or mt3) in this region almost completely abrogated ETV2 responsiveness in the luciferase activity (Fig 5D). Collectively, we conclude that ETV2 positively regulates its own expression and that of other *Ets* genes.

Having confirmed that *Ets* genes are ETV2 targets, we validated the kinetics of the *Ets* gene expression in developing EBs and embryos. Indeed, *Etv2* expression precedes that of other *Ets* genes in differentiating ES cells. Specifically, *Fli1* expression was detected shortly after *Etv2*, followed by *Erg*, *Elk3, Ets1,* and *Ets2* (Fig 6A). Moreover, in the DOX-inducible *Etv2* expression system (*iEtv2* ES), where *Etv2* expression becomes visible within 6 h of DOX addition, expression *of Fli1*, *Erg,* and *Elk3* was prominently induced by 12–24 h after DOX addition (Fig 6B). *Ets1* and *Ets2* were also induced, although at much modest levels (Fig 6B). Importantly, expression of *Fli1*, *Erg,* and *Elk3* was greatly reduced in *Etv2*-null embryos (Fig 6C). Expression *of Ets1* and *Ets2* was also reduced in *Etv2*-null embryos (Fig 6C). If *Fli1* is truly a direct target of *Etv2* in hematopoietic and endothelial cell development, it was expected that *Etv2* expression would be unaffected by *Fli1* manipulation. Indeed, expression *of Etv2*, *Erg,* and *Elk3* was not impaired in *Fli1*-null ES cells differentiated in culture (Fig 6D) or in embryos (Fig 6E). Moreover, enforced *Fli1* expression in differentiating ES cells (*iFli1* ES cells) did not alter *Etv2* expression, although other *Ets* genes were upregulated (Fig 6F).

Hierarchical ETS function in hemangioblast, hematopoietic, and endothelial cell lineage development

One possibility for the non-redundant role of ETV2 in the $FLK1^{high}PDGFR\alpha^{-}$ hemangioblast commitment could be the timing of the ETS factor availability. As such, ETV2 happens to be expressed before the other ETS factors and thus carries out such a robust function. To determine whether ETS factors are inherently redundant or unique in their function in the hematopoietic and endothelial cell specification, we analyzed the hemangiogenic output by *Fli1*, the immediate ETV2 target. Specifically, we determined whether $Fli1^{-/-}$ embryos showed defects in the $FLK1^{+}PDGFR\alpha^{-}$ hemangiogenic progenitor generation. As shown, $FLK1^{high}PDGFR\alpha^{-}$ progenitor cell population still developed in the *Fli1*-null embryos and ES cells, similar to wild-type control levels, suggesting that hemangioblast formation does not require FLI1 function (Fig 7A and B, Supplementary Fig S4A and B). However, enforced *Fli1* expression was able to skew mesoderm, although at a lesser degree than ETV2, into the hemangiogenic fate in *iFli1* ES cells (Fig 7C and Supplementary Fig S4C). *Ets1* or *Ets2* cannot skew mesoderm into the hemangioblast [39]. This supports the notion that *Fli1* is not necessary, but sufficient for hemangioblast generation. *Ets1* or *Ets2* cannot induce hemangioblast, even if overexpressed at the same time frame as *Etv2*.

To further elicit functional hierarchy among ETS factors, we additionally determined the hemangioblast skewing effect by different ETS factors in the context of *Gata2* and *Scl* coexpression. We previously reported that *Etv2,* when coexpressed with *Gata2* and *Scl*, robustly skewed mesoderm toward the hemangioblast while suppressing the cardiac output from ES cells [39]. Thus, we compared the coexpression effect of *Ets* genes with *Gata2* and *Scl* on the $FLK1^{+}PDGFR\alpha^{-}$ hemangioblast formation. We specifically generated doxycycline-inducible ES cells coexpressing *Fli1-Gata2-Scl*, *Erg-Gata2-Scl,* or *Ets1-Gata2-Scl.* As previously reported [39], *Etv2-Gata2-Scl* coexpression during mesoderm formation stage robustly induced $FLK1^{+}PDGFR\alpha^{-}$ hemangioblast from ES cells. While $FLK1^{+}PDGFR\alpha^{-}$ hemangioblast population was increased by *Fli1-Gata2-Scl* or *Erg-Gata2-Scl*, the level of the $FLK1^{+}PDGFR\alpha^{-}$

 © 2015 The Authors

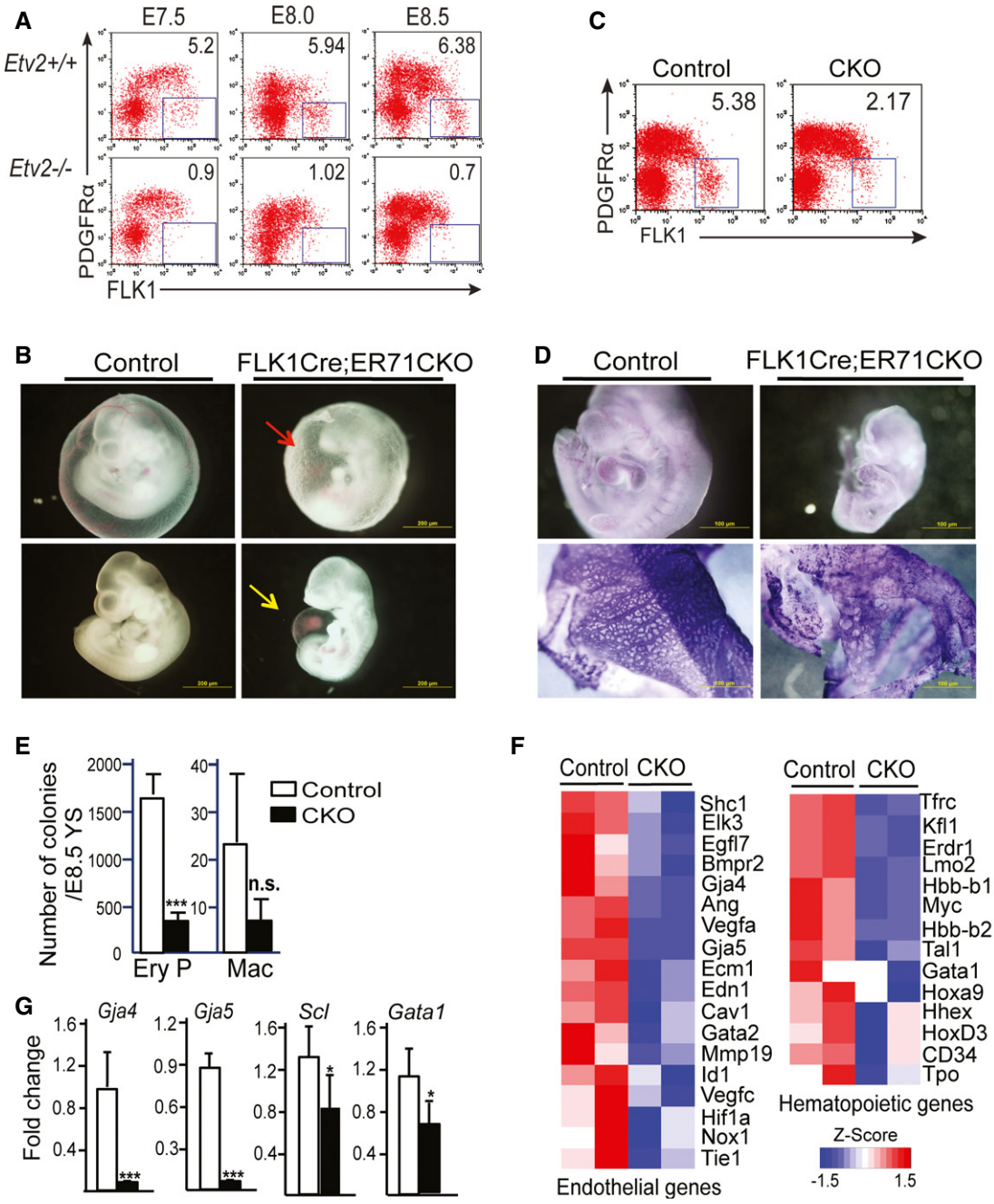

Figure 4. ETV2 is required for the generation and expansion of hemangioblast.

A *Etv2*$^{+/+}$ and *Etv2*$^{-/-}$ yolk sac and embryo proper were analyzed for FLK1 and PDGFRα expression at E7.5, 8, and 8.5 (n = 6 for each). Representative FACS analysis at each time point is shown.

B Gross morphology of the E10.5 *Flk1Cre;Etv2* CKO embryos is shown. Note the wrinkled yolk sac (red arrow) and the swollen pericardial cavity accumulated with fluid/blood (yellow arrow) in the mutants.

C FACS analysis of E8.5 *Flk1Cre;Etv2* CKO embryos for FLK1 and PDGFRα expression.

D CD31/PECAM1 whole-mount staining of the E9.5 embryos (up: embryos; down: yolk sacs).

E Hematopoietic colony assay of the E8.5 wild-type and mutant yolk sacs. Mean ± SD, n = 4 biological replicates. ***$P < 0.001$, two-tailed Student's t-test.

F, G Microarray analysis (F) and qRT–PCR analysis (G) of the *Flk1Cre;Etv2* CKO yolk sacs. Mean ± SD, n = 3 biological replicates. *$P < 0.05$, ***$P < 0.001$, two-tailed Student's t-test.

cells generated by *Fli1-Gata2-Scl* or *Erg-Gata2-Scl* was not as robust as that by the *Etv2-Gata2-Scl* (Fig 7D, Supplementary Fig S4D). Importantly, there was incomplete skewing of mesoderm toward FLK1^{+}PDGFRα^{-} hemangioblast by *Fli1-Gata2-Scl* or *Erg-Gata2-Scl*, as judged by FLK1^{+}PDGFRα^{+} cardiac mesoderm production (Fig 7D, Supplementary Fig S4D). *Ets1-Gata2-Scl* was

© 2015 The Authors

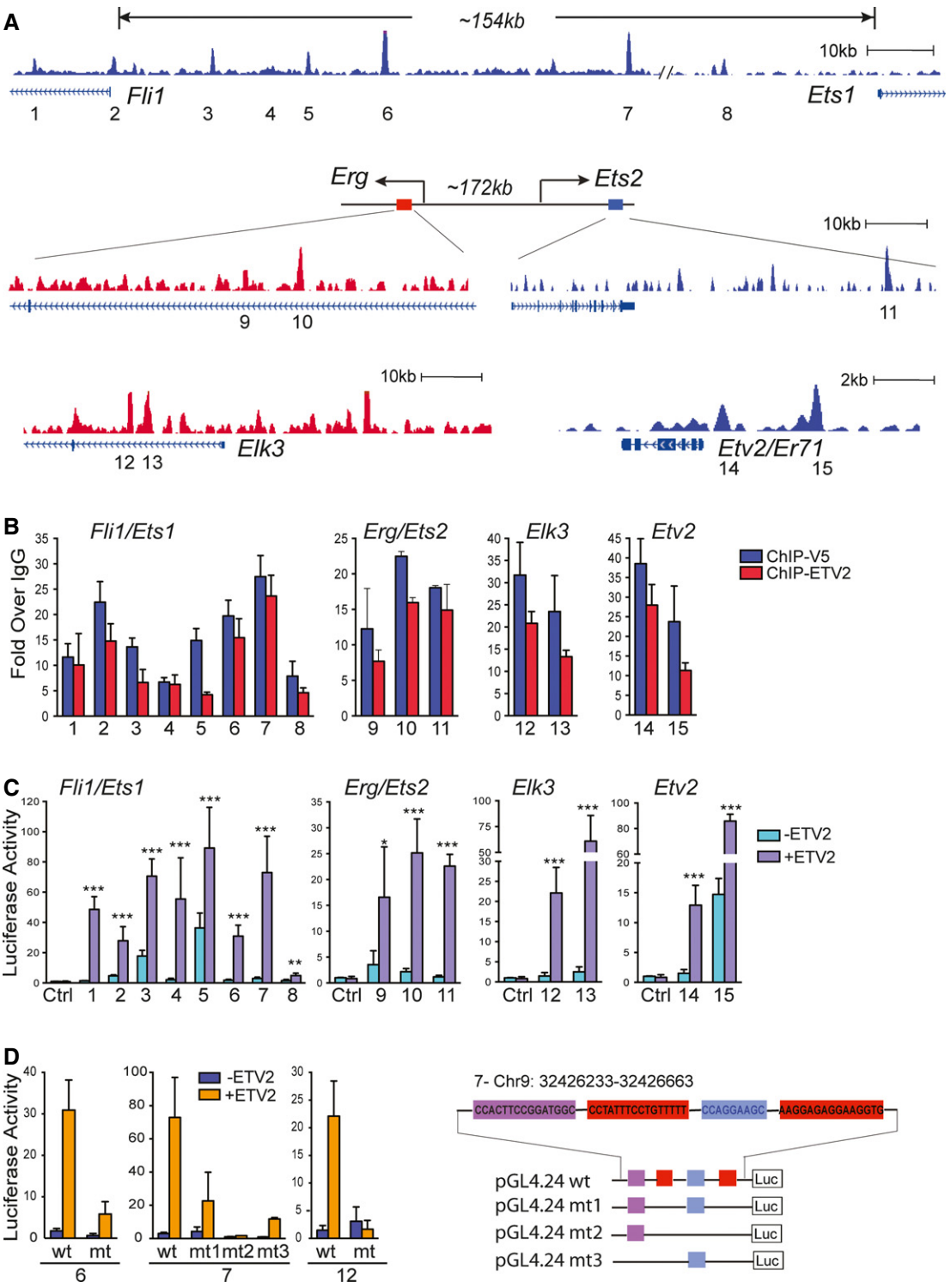

Figure 5. *Ets* genes are direct targets of ETV2.

A Genome browser views of the ETV2 binding peaks associated with Ets loci. Numbers (1–15) indicate ETV2 peaks.

B ETV2 enrichment at ETV2 peaks (1–15) by ChIP-qPCR analysis (mean ± SD, n = 4 biological replicates). PCR primers and genomic locations are provided in Supplementary Table S3.

C Luciferase reporter assay for 1–15 ETV2 peak regions from (A). Similar to Fig 3C, the graph shows relative luciferase activity over reporter construct alone in the presence or absence of ETV2 expression plasmids (pMSCV-*Etv2*). Data are represented as mean + SEM. n = 4. *P < 0.05; **P < 0.01; ***P < 0.001, two-tailed Student's t-test.

D Luciferase reporter assay for the deletion mutants of the ETV2 motif in the selected peak regions (6, 7, and 12) is shown on the left (see Supplementary Table S3). Deletions of 2 (mt1, mt2) or 3 (mt3) ETV2 motifs within the peak 7 are shown on the right. Error bars represent the SEM obtained from four biological replicates.

 © 2015 The Authors

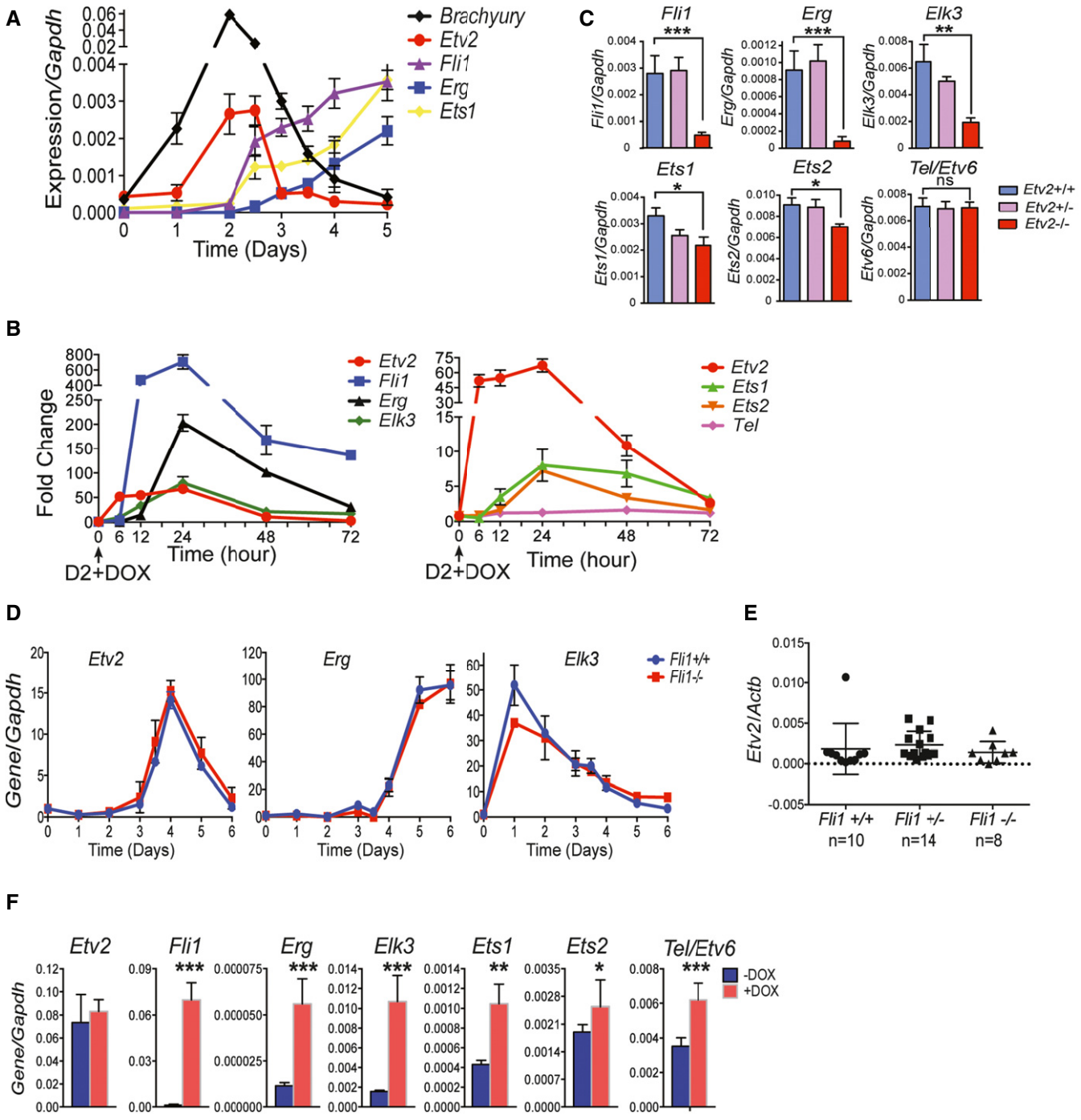

Figure 6. ETV2 functions at the top of the ETS hierarchy in development.

A Kinetic analysis of *Brachyury* and *Ets* gene expression in wild-type EBs, day 0 to day 5, is shown. Gene expression was normalized to *Gapdh*. Error bars represent the SD from four independent experiments.

B Inducible *Etv2* ES cells were differentiated in serum-free conditions with DOX added on day 2. *Ets* gene expression was analyzed at indicated times by qRT–PCR. Mean ± SD, $n = 4$ biological experiments. Genes were normalized to *Gapdh*, and the ratio of the +DOX gene quantity to −DOX gene quantity was determined to yield fold changes shown on the *y*-axis.

C qRT–PCR analysis of *Ets* gene expression in E8.5 embryos of $Etv2^{+/+}$ ($n = 10$), $Etv2^{+/-}$ ($n = 18$) and $Etv2^{-/-}$ ($n = 9$) (embryos were obtained from 4 to 5 pregnant mice). Gene expression was normalized to *Gapdh*. Mean values are shown ± SD. Student's *t*-test *$P < 0.05$; **$P < 0.01$; ***$P < 0.001$; ns, not significant.

D $Fli1^{+/+}$ and $Fli1^{-/-}$ ES cells were differentiated on OP9 feeder cells and the expression of *Etv2*, *Erg*, and *Elk3* genes was analyzed from day 0 to day 6. Mean ± SD, $n = 4$ experiments.

E Analysis of *Etv2* expression in E8.5 embryos of $Fli1^{+/+}$ ($n = 10$), $Fli1^{+/-}$ ($n = 14$) and $Fli1^{-/-}$ ($n = 8$) (embryos were obtained from 4 to 5 pregnant mice). Gene expression was normalized to *β-actin*. Mean values are shown ± SD.

F Expression of *Ets* genes was analyzed on day 3 *iFli1* EB cells with DOX added on day 2 (mean ± SD, $n = 4$). Student's *t*-test *$P < 0.05$; **$P < 0.01$; ***$P < 0.001$.

© 2015 The Authors

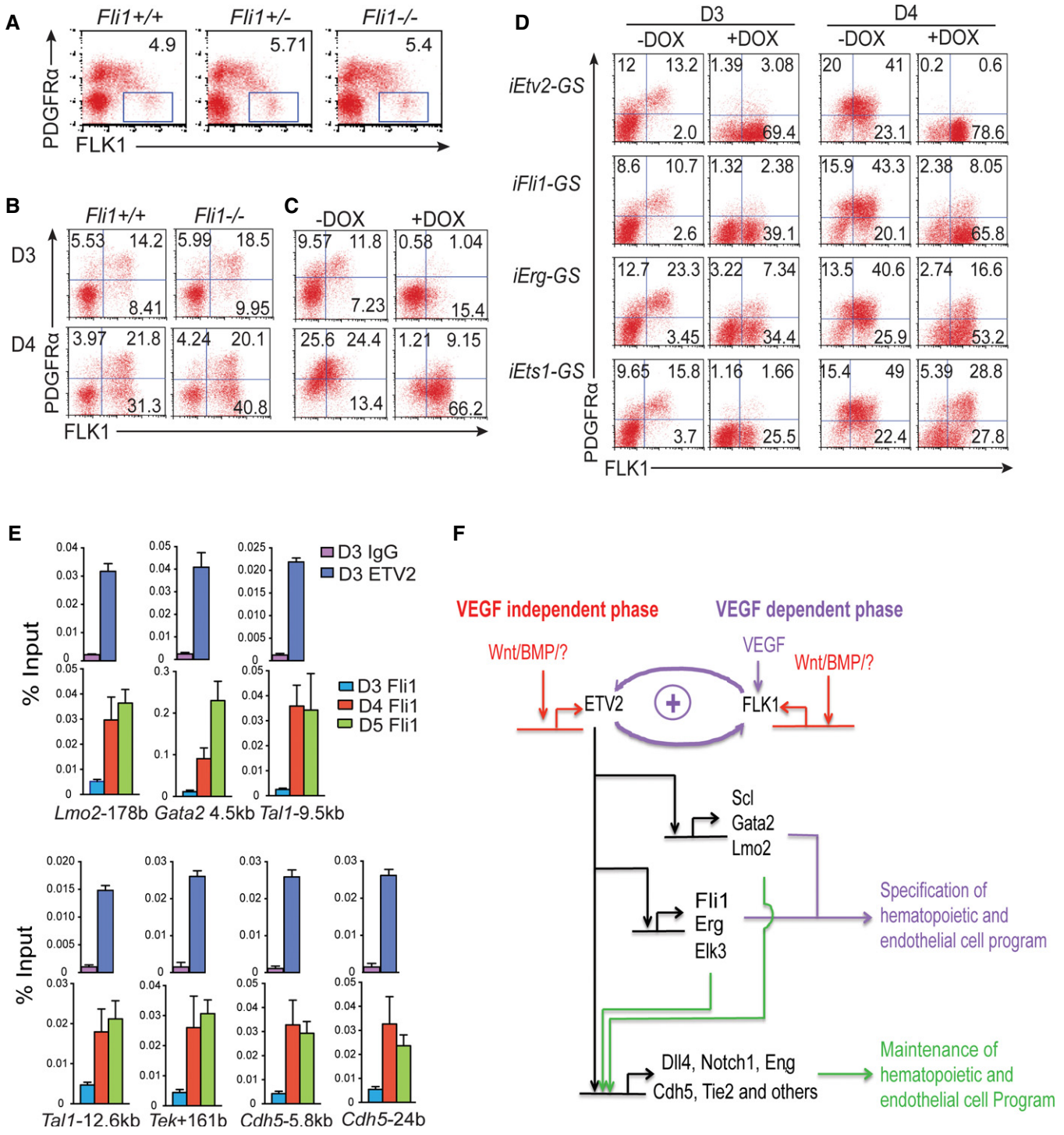

Figure 7. ETS switching mechanism in maintaining hematopoietic and endothelial cell program.

A–C A representative FACS profile of FLK1 and PDGFRα expression of E8.5 *Fli1*$^{+/+}$ (n = 9), *Fli1*$^{+/-}$ (n = 11), and *Fli1*$^{-/-}$ (n = 6) embryos (A) (embryos were obtained from 4 to 5 pregnant mice); *Fli1*$^{+/+}$ and *Fli1*$^{-/-}$ EBs (B, four independent biological samples); and *iFli1* EBs (± DOX) (C, four independent biological samples) at indicated times.

D *iEtv2-GS* (=*iEtv2-2A-Gata2-2A-Scl*), *iFli1-GS*, *iErg-GS*, and *iEts1-GS* EBs were treated with DOX from day 2 and analyzed for FLK1 and PDGFRα at indicated times. Numbers indicate the percentage within each quadrant. Representative results from four independent biological samples are shown.

E The enrichment of ETV2 and FLI1 binding at the indicated gene loci by ChIP-qPCR analysis in wild-type EBs is shown. qPCR primers and genomic locations are provided in Supplementary Table S3. Error bars represent SD, n = 4. *P < 0.05, **P < 0.01, ***P < 0.001 by Student's two-tailed t-test.

F A model showing ETV2 regulation of the hematopoietic and endothelial cell program.

© 2015 The Authors

least effective in inducing FLK1^{+}PDGFRα^{-} hemangioblast from ES cells (Fig 7D, Supplementary Fig S4D). Collectively, ETV2 carries out a uniquely distinct role in the hemangioblast generation. No other ETS factors can replace ETV2 in the hemangioblast formation.

Hematopoietic and endothelial cell program is maintained by an ETS switching mechanism

ETV2 ChIP-Seq identified key hematopoietic and endothelial cell genes as ETV2 direct targets. However, the mechanism that allows these genes to be continuously expressed in mature hematopoietic and endothelial cells even when *Etv2* is no longer expressed remains to be elucidated. We postulated that ETV2 target gene expression could be maintained within mature hematopoietic and endothelial cells by other ETS factors, which were induced by ETV2. To this end, we analyzed key target genes, *Lmo2*, *Gata2*, *Cdh5*, *Tie2/Tek*, and *Scl/Tal1* for the ETS factor occupancy using day 3 and day 4–5 EB cells. Specifically, we hypothesized that while the ETS sites of the target genes would be occupied by ETV2 in days 2–3 EBs, when ETV2 expression is robust, the same target sites would be occupied by other ETS factors when ETV2 is no longer expressed, that is, days 4–5. To test this idea, we collected wild-type EB cells at day 3, 4, and 5 and performed ChIP-qPCR using ETV2-polyAbs and FLI1 Ab. As shown, while the evolutionary conserved potential ETS binding sites of these genes were occupied by ETV2 in day 3 EBs, the same regions were occupied by FLI1 in later developmental stages, that is, days 4 and 5. FLI1 occupancy on these genes was minimal in day 3 EBs (Fig 7E). Collectively, ETV2-initiated blood and endothelial cell program is maintained by other ETS factors through an ETS switching mechanism.

Discussion

Studies so far have established a non-redundant and essential function of ETV2 in blood and vascular development. However, mechanistic understanding of how ETV2 performs such a profound function in blood and vessel formation has been lacking. We demonstrate that FLK1^{high}PDGFRα^{-} cell population enriched for hemangiogenic progenitors is uniquely sensitive to ETV2 function, as this population was specifically missing in *Etv2*-deficient embryos. The formation of the FLK1^{high}PDGFRα^{-} cell population would require simultaneous activation of the hematopoietic and endothelial cell lineage specifying genes and FLK1 signaling, which are coordinated by ETV2. As *Flk1Cre;Etv2CKO* mice generate suboptimal levels of FLK1^{high}PDGFRα^{-} progenitor, we propose that ETV2 is required up to the timeframe when FLK1^{high}PDGFRα^{-} hemangiogenic progenitor population is sufficiently generated to ensure proper hematopoietic and endothelial cell generation. Based on studies that VEGF-FLK1 signaling can induce *Etv2* expression [26,43], we propose that ETV2-FLK1 feed forward mechanism is responsible for FLK1^{high}PDGFRα^{-} hemangiogenic progenitor expansion (Fig 7F). Collectively, we provide novel insights into how the FLK1^{high}PDGFRα^{-} hemangiogenic progenitor specification is achieved by ETV2.

Consistent with our data that *Etv2* was still required downstream of *Flk1*, *Etv2* deletion using tamoxifen injection from E8.5, but not E9.5, in ROSACreER;*Etv2*$^{f/f}$ mice results in similar vascular development defects as ours [44]. Intriguingly, *Flk1Cre;Etv2 CKO* mice were reported to be born without any phenotypic defects [35]. Given that *Etv2* expression is transient and that *Etv2* deletion using the *Tie2-Cre* or tamoxifen injection in ROSACreER;*Etv2*$^{f/f}$ mice from E9.5 leads to normal live birth [44], the discrepancy in the embryonic lethality between the two studies might be due to different deletion efficiency or the accessibility of the floxed *Etv2* alleles. For example, while exons 5–6 were floxed in our study, the entire *Etv2* gene was floxed in the reported study, which might have contributed to different CRE accessibility of the floxed alleles in the chromatin context. We rule out the possibility that our strategy might have generated a dominant negative protein and contributed to the embryonic lethal phenotype, since *Etv2* message corresponding to exons 2–3 in purified endothelial cells (CD45^{-}CD31^{+}) from the *Tie2Cre;Etv2*$^{f/-}$ (or *Tie2Cre;Etv2*$^{f/f}$) mice was virtually undetectable (not shown). Additionally, genetic backgrounds often affect the severity of the knockout phenotypes. In our studies, *Flk1Cre*, *Etv2*$^{+/-}$, and *Etv2*$^{fl/f}$ mice have all been backcrossed to and maintained on a pure C57BL/6 background.

As ETV2 function is transiently required, there must be a mechanism maintaining the hematopoietic and endothelial cell program that was initiated by ETV2. We propose that ETV2 drives lineage-specific epigenetic landscape in blood and vascular systems. As ETV2 target loci remained unmethylated in the heart and bone marrow (Fig 2B and Supplementary Fig S1G), ETV2 binding could directly result in demethylation of its binding sites, thereby shaping the lineage-specific epigenome [33]. Hypomethylation of these binding sites is maintained in blood and vascular systems as an epigenetic memory [45], potentially serving as the future tissue-specific enhancer elements of ETV2 downstream factors. We provide ETS switching mechanism as one such mode. Similar to the GATA switching mechanism controlling the erythroid cell lineage differentiation [46,47], ETV2 induces expression of other *Ets* genes, thereby creating an ETS hierarchy. Specifically, we show that hematopoietic and endothelial cell program is initiated by ETV2, but is maintained by other ETS factors (Fig 7F). However, timing of different *Ets* factor expression alone cannot explain the non-redundant ETV2 function, as we demonstrated that FLI1, ERG, or ETS1 could not replace ETV2 function even if they were expressed at the same time frame as ETV2, in the hemangioblast induction from ES cells. To this end, structure and function of ETV2 in relationship to other ETS factors may elucidate the unique role of ETV2 in the hematopoietic and endothelial cell development. Additionally, ETV2 may require a unique cofactor(s). Recent finding of OVOL2 as ETV2, not ETS1 or ETS2, cofactor further suggests such non-redundant function played by ETV2 [48].

While ETV2 is a potent inducer of the hemangiogenic program, it is transiently expressed, suggesting that there might be a strong pressure to keep this gene off once hematopoietic and vascular systems are established. Indeed, sustained *Etv2* expression during development results in hematopoietic and vessel defects as manifested by dilated yolk sac vessels [49]. Future studies on *Etv2* gene regulation are warranted. Presumably, *Etv2* reactivation in mature endothelial cells might be a helpful strategy for hematopoietic and endothelial cell regeneration or diseases requiring angiogenesis, such as peripheral arterial disease and wound healing. To this end, it is worth noting that *Etv2*, alone or in combination with other endothelial cell factors, can reprogram somatic cells to functional

© 2015 The Authors

endothelial cells [50,51]. It will also be important to determine whether *Etv2* is aberrantly expressed in pathologic conditions, such as tumor angiogenesis. If so, mechanisms involved in *Etv2* down-regulation may have a direct efficacy in the pathologic angiogenesis.

Materials and Methods

Antibodies

Antibodies against V5 (ab15828), control rabbit IgG (ab31475), and FLI1 (ab15289) were purchased from Abcam (Cambridge, MA). Polyclonal antibodies against endogenous ETV2 (ETV2-polyAbs) were produced by YenZym Antibodies (South San Francisco, CA). Briefly, rabbits were immunized three times with a synthetic peptide corresponding to the mouse $ETV2_{200–219}$ (EGHQSPAFTTPSKSNKQ SDR). Polyclonal antibody was affinity purified using ETV2 peptide-conjugated affinity matrix. Antibody specificity was further confirmed by antigen-specific ELISA and immunoprecipitation followed by Western blot.

Knockout and conditional knockout mouse analysis

Heterozygous $Etv2^{+/-}$ or $Fli1^{+/-}$ mice were subjected to brother–sister matings to generate $Etv2^{-/-}$ or $Fli1^{-/-}$ embryos. *Flk1Cre;Etv2* CKO mice were generated by crossing $Flk1^{+/Cre}$;$Etv2^{+/-}$ (or $Flk1^{+/Cre}$;$Etv2^{f/+}$) and $Etv2^{f/f}$ mice. The generation of *Flk1Cre*, $Etv2^{+/-}$, $Etv2^{f/f}$, and $Fli1^{+/-}$ mice has been previously described [20,24,52,53]. Information on genotyping primers was previously described [24,27,38,39]. Embryos from E7.5 to E9.5 were dissected and disassociated with 0.1% trypsin for 5 min or 0.25% collagenase for 30 min at 37°C into single cells and then subjected to FACS analysis or RNA extraction using RNeasy micro Kit (Qiagen) for gene expression. All mouse experiments were done in accordance with protocols approved by the Institutional Animal Care and Use Committee of Washington University in St. Louis Medical School.

ES cell generation and differentiation

$Fli1^{-/-}$ ES cells were generated from blastocysts obtained from the $Fli1^{+/-}$ brother–sister matings. Inducible ES cell lines (*iEtv2 and iEGS)* were previously described [24,27,37,38]. Inducible *Fli1 (iFli1)* ES cells were generated by targeting *Fli1* into the tet-responsive locus of A2Lox cells [38]. To generate inducible *Fli1-2A-Gata2-2A-Scl* (*iFli1-GS*), *Erg-2A-Gata2-2A-Scl* (*iErg-GS*), or *Ets1-2A-Gata2-2A-Scl* (*iEts1-GS*) ES cells, coding sequence of *Ets (Fli1, Erg* and *Ets1)*, *Gata2,* and *Scl*, linked by 2A peptides [54], were targeted into the tet-responsive locus of A2 Lox cells. The correct targeting event was confirmed by a tet-responsive locus/cDNA vector-specific PCR. Doxycycline (DOX) was typically added to the differentiating ES cells from day 2 to induce the genes.

Chromatin immunoprecipitation (ChIP)-sequencing

Wild-type or *iEtv2* EBs from day 3–5 were subjected to ChIP assay. Briefly, EBs were disassociated into single cells by trypsin, fixed with 1% formaldehyde at room temperature for 10 min, and quenched by adding glycine to 125 mM final concentration. The cross-linked cell pellets ($1–2 \times 10^7$) were resuspended in lysis buffer (1% SDS, 5 mM EDTA, 50 mM Tris–HCl [pH 8.1], plus protease inhibitor) and gently rocked at 4°C for 10 min, then sonicated to 200- to 600-bp fragments using an AFA Focused-ultrasonicator or a Diagenode Bioruptor. Sonicated lysates were cleared by pelleting insoluble material at $20{,}000 \times g$ for 20 min at 4°C. The soluble lysate was diluted by adding 9 volumes of IP buffer (1% Triton X-100, 2 mM EDTA, 150 mM NaCl, 20 mM Tris–HCl [pH 8.1], 1× protease inhibitor cocktail). Subsequently, the lysate was precleared with 30 μl of protein A- or G- Sepharose beads for 2 h at 4°C under rocking, followed by incubation with specific antibody overnight at 4°C. Subsequently, 45 μl protein A- or G- Sepharose beads were added and incubated for 2–3 h at 4°C. The beads were then washed three times serially with cold wash buffer TSE I (0.1% SDS, 1% Triton X-100, 2 mM EDTA, 20 mM Tris–HCl, pH 8.1, 150 mM NaCl), TSE II (0.1% SDS, 1% Triton X-100, 2 mM EDTA, 20 mM Tris–HCl, pH 8.1, 500 mM NaCl), buffer III (0.25 M LiCl, 1% NP-40, 1% deoxycholate, 1 mM EDTA, 10 mM Tris–HCl, pH 8.1) and then TE buffer. Precipitated chromatin complexes were eluted in 100 μl elution buffer (1% SDS, 0.1 M $NaHCO_3$) at room temperature for 10 min and uncross-linked overnight at 65°C, followed by RNase A treatment for 2 h and then proteinase K for 2 h. DNA was extracted with QiaQuick PCR purification kit (Qiagen).

Immunoprecipitated DNA yield was determined via Quant IT fluorescence assay (Invitrogen), and transcription factor enrichment was evaluated by qPCR. Illumina sequencing libraries were generated as following. ChIP DNA was blunt-ended, "A" base was added to 3′ end, and sequencing adapters were ligated to the ends. The fragments were size-selected to 200–600 base pairs and underwent amplification for 15 cycles. The resulting libraries were sequenced using the Illumina HiSeq-2000 as single reads extending 50 bases. The raw data were demultiplexed and aligned to the reference genome using Bowtie. MACS was used to call peaks.

Sequence alignment and peak calling

Sequences reads were submitted to NCBI Gene Expression Omnibus (GEO; http://www.ncbi.nlm.nih.gov/geo/) under Accession Number GSE59402. Sequence reads were aligned to mouse genome assembly mm9 [28] using BWA aligner [55] for alignment and methylQA [56] for initial process. MACS2 [29] was used for peak calling against IgG input using *P*-value threshold 1E-6.

GREAT analysis

Peak regions were submitted to GREAT (http://bejerano.stanford.edu/great/public/html/, version 2.0.2) using default "Basal plus extension" settings. Enrichment terms less than FDR threshold 0.05 were regarded as statistical significant.

Motif analysis

The ETV2 motif was *de novo* trained from peaks we identified using Homer software [57]. We also used Homer for motif scanning on peak regions. Statistic tests were performed using R environment (http://www.r-project.org/). ETV2 and GATA2 motif came from the *de novo* training results; SCL (E-box) motif was generated using

 © 2015 The Authors

seq2profile.pl utility from Homer software using consensus sequence CANNTG. Homer was also used for motif scanning in peaks. Peaks with all 3 motifs occurring were used for calculating the nearest distance of ETV2-SCL and SCL-GATA2 using custom script. The ETV2-SCL-GATA2 logo was generated by WebLogo 3 (http://weblogo.threeplusone.com/create.cgi).

Microarray analysis

We analyzed microarray data following instructions as previously described [58]. Genes shown 1.5-fold downregulated in *Etv2* knock out and DOX+ upregulated, or 1.5-fold upregulated in *Etv2* knock out and DOX+ downregulated were used to overlap with genes identified from ChIP-Seq experiments.

RNA obtained from controls and *Flk1Cre;Etv2CKO* E9.5 yolk sacs was used to gene expression profiling analyses with Illumina MouseWG-6 v2.0 Expression BeadChip Kits at the Northwestern University Genomic Core, Chicago.

Evolutionary analysis

The 30-way vertebrate alignment conservation data were downloaded from UCSC Genome Browser; for each peak, we extend 3 kb from the peak center and split this 6-kb region to 50-bp bins, we assigned each bin with an average conservation score using custom script.

Analysis of whole-genome bisulfite sequencing data

We downloaded published whole-genome bisulfite sequencing (WGBS) data from GEO [33,34] and assigned the CpG sites around 6-kb region centered each peak center with methylation values for these tissues including ESC (GSE30202), heart (GSM1051154), bone marrow (GSM1051150), neuronal progenitors (GSE30202), and cerebellum (GSM1051151). These 6-kb regions were split to 50-bp bins, and methylation values for each bin were averaged from all ChIP-Seq peaks. Profile of peaks, which were distal (> 1 kb distance) to nearest TSS, was plotted, and a generalized linear model was applied to smooth the methylation changes.

Luciferase reporter assay

ETV2 bound sequences (Supplementary Table S3) obtained through MACS peak-calling algorithm were PCR-amplified and cloned into the pGL4.24[*luc2*P/minP] vector containing the minimal promoter and the luciferase reporter gene *luc2P*. Selected peak regions containing ETV2 binding motif were deleted as shown in Supplementary Table S3. For luciferase assays, 293T cells cultured in DMEM supplemented with 10% fetal bovine serum were plated onto 24-well plates (3×10^4 cells) and transfected the next day with the various pGL4.24[*luc2*P/minP] vector constructs with or without the ETV2 expression plasmid (pMSCV-*Etv2*). Renilla luciferase vector (Promega) was cotransfected to normalize transfection efficiency. Transfection was performed using Lipofectamine 2000 (Invitrogen, Carlsbad, CA). Cells were harvested 48 h after transfection, and luciferase activity was measured using the Dual-Luciferase Reporter Assay kit and GloMax™ Systems (Promega). Reporter gene activities were first normalized to the Renilla luciferase value and further compared to that of the control pGL4.24 reporter. All experiments were repeated four biological replicates.

Flow cytometry

Embryoid bodies (EBs) or mouse embryos were harvested and dissociated into single cells using 0.1% trypsin (EBs) or 0.25% collagenase (embryos) for staining. Primary Abs included biotin-α-FLK1 (1:200, Avas12, BioLegend), APC-α-PDGFRα (1 μg/ml, APA5, eBioscience), and PE-α-CD31 (1 μg/ml, MEC13.3, Biolegend). Streptavidin (SA)/PE (0.5 μg/ml, eBioscience) was used as secondary antibody. Data were acquired on a FACSCalibur flow cytometer (Becton Dickinson) and analyzed using FlowJo (Treestar) software.

Signaling pathway RT^2 profiler PCR array

The RT^2 Profiler PCR Array that profiles the expression of 84 key genes in the mouse VEGF signaling (PAMM-091ZA) and the Cell Motility (PAMM-128ZA) pathway were purchased from SA-Bioscience (Qiagen). Total RNA was isolated from day 3.5 *iEtv2* EBs (±DOX on day 2–3.5) and a pool of E8.5 $Etv2^{+/+}$ or $Etv2^{-/-}$ embryos, converted to cDNAs, and used for screening by real-time PCR following the manufacturer's instructions. qRT–PCR assays performed in triplicate, normalized to 4 housekeeping genes (*Gusb*, *Hsp90ab1*, *Gapdh,* and *Actb*), and analyzed according to the $\Delta\Delta C_T$ method with the SA-Biosciences proprietary software.

Quantitative real-time reverse transcription PCR (qRT–PCR)

Total RNA from embryos and EB cells were prepared with RNeasy Micro/Mini Kit, and reverse-transcribed into cDNAs according to manufacturer's protocol. Expression of genes was measured by quantitative real-time RT–PCR with primers indicated in Supplementary Table S6. Gene expression levels were normalized to *Gapdh* or *β-actin*.

Statistical analysis

Student's *t*-test (Prism5, GraphPad Software, La Jolla, CA) was used for statistical analysis. A *P*-value of < 0.05 was considered as significant.

Supplementary information for this article is available online: http://embor.embopress.org

Acknowledgements

This work was supported by grants from the National Institutes of Health, NHLBI, HL63736, and HL55337 (K.C.); NHGRI, HG007354, HG007175, ES024992 (T.W.); American Cancer Society, RSG-14-049-01-DMC (T.W.); HL119291 (C.P.); American Heart Association, 11SDG7390074 (C.P.); the March of Dimes Foundation, #5-FY12-44 (C.P.).

Author contributions

FL and KC conceived the experiments, analyzed the data, and wrote the manuscript. FL, YY, IK, and MC performed experiments. JK and CP performed *Etv2* conditional knockout studies. DW provided *Fli1* knockout mice. DL and TW performed bioinformatics analysis and wrote the manuscript.

© 2015 The Authors

Conflict of interest

The authors declare that they have no conflict of interest.

References

1. Choi K, Kennedy M, Kazarov A, Papadimitriou JC, Keller G (1998) A common precursor for hematopoietic and endothelial cells. *Development* 125: 725 – 732
2. Murray PDF (1932) The development in vitro of the blood of the early chick embryo. *Proc Roy Soc London* 11: 497 – 521
3. Nishikawa SI, Nishikawa S, Hirashima M, Matsuyoshi N, Kodama H (1998) Progressive lineage analysis by cell sorting and culture identifies FLK1+VE-cadherin+ cells at a diverging point of endothelial and hemopoietic lineages. *Development* 125: 1747 – 1757
4. Sabin FR (1920) Studies on the Origin of Blood-vessels and of Red Blood-corpuscles as Seen in the Living Blastoderm of Chicks During the Second Day of Incubation. *Contrib Embryol* 9: 213 – 262
5. Padron-Barthe L, Temino S, Villa del Campo C, Carramolino L, Isern J, Torres M (2014) Clonal analysis identifies hemogenic endothelium as the source of the blood-endothelial common lineage in the mouse embryo. *Blood* 124: 2523 – 2532
6. Myers CT, Krieg PA (2013) BMP-mediated specification of the erythroid lineage suppresses endothelial development in blood island precursors. *Blood* 122: 3929 – 3939
7. Bertrand JY, Chi NC, Santoso B, Teng S, Stainier DY, Traver D (2010) Haematopoietic stem cells derive directly from aortic endothelium during development. *Nature* 464: 108 – 111
8. Boisset JC, van Cappellen W, Andrieu-Soler C, Galjart N, Dzierzak E, Robin C (2010) In vivo imaging of haematopoietic cells emerging from the mouse aortic endothelium. *Nature* 464: 116 – 120
9. Kissa K, Herbomel P (2010) Blood stem cells emerge from aortic endothelium by a novel type of cell transition. *Nature* 464: 112 – 115
10. Lam EY, Hall CJ, Crosier PS, Crosier KE, Flores MV (2010) Live imaging of Runx1 expression in the dorsal aorta tracks the emergence of blood progenitors from endothelial cells. *Blood* 116: 909 – 914
11. Butler JM, Nolan DJ, Vertes EL, Varnum-Finney B, Kobayashi H, Hooper AT, Seandel M, Shido K, White IA, Kobayashi M *et al* (2010) Endothelial cells are essential for the self-renewal and repopulation of Notch-dependent hematopoietic stem cells. *Cell Stem Cell* 6: 251 – 264
12. Kiel MJ, Yilmaz OH, Iwashita T, Terhorst C, Morrison SJ (2005) SLAM family receptors distinguish hematopoietic stem and progenitor cells and reveal endothelial niches for stem cells. *Cell* 121: 1109 – 1121
13. Morrison SJ, Scadden DT (2014) The bone marrow niche for haematopoietic stem cells. *Nature* 505: 327 – 334
14. Shalaby F, Rossant J, Yamaguchi TP, Gertsenstein M, Wu XF, Breitman ML, Schuh AC (1995) Failure of blood-island formation and vasculogenesis in Flk-1-deficient mice. *Nature* 376: 62 – 66
15. Carmeliet P, Carver-Moore K, Chen H, Dowd M, Lu L, O'Shea KS, Powell-Braxton L, Hillan KJ, Moore MW (1996) Abnormal blood vessel development and lethality in embryos lacking a single VEGF allele. *Nature* 380: 435 – 439
16. Ferrara N, Carver-Moore K, Chen H, Dowd M, Lu L, O'Shea KS, Powell-Braxton L, Hillan KJ, Moore MW (1996) Heterozygous embryonic lethality induced by targeted inactivation of the VEGF gene. *Nature* 380: 439 – 442
17. De Val S, Chi NC, Meadows SM, Minovitsky S, Anderson JP, Harris IS, Ehlers ML, Agarwal P, Visel A, Xu SM *et al* (2008) Combinatorial regulation of endothelial gene expression by ets and forkhead transcription factors. *Cell* 135: 1053 – 1064
18. Wythe JD, Dang LT, Devine WP, Boudreau E, Artap ST, He D, Schachterle W, Stainier DY, Oettgen P, Black BL *et al* (2013) ETS factors regulate Vegf-dependent arterial specification. *Dev Cell* 26: 45 – 58
19. Oikawa T, Yamada T (2003) Molecular biology of the Ets family of transcription factors. *Gene* 303: 11 – 34
20. Spyropoulos DD, Pharr PN, Lavenburg KR, Jackers P, Papas TS, Ogawa M, Watson DK (2000) Hemorrhage, impaired hematopoiesis, and lethality in mouse embryos carrying a targeted disruption of the Fli1 transcription factor. *Mol Cell Biol* 20: 5643 – 5652
21. Pham VN, Lawson ND, Mugford JW, Dye L, Castranova D, Lo B, Weinstein BM (2007) Combinatorial function of ETS transcription factors in the developing vasculature. *Dev Biol* 303: 772 – 783
22. Abedin MJ, Nguyen A, Jiang N, Perry CE, Shelton JM, Watson DK, Ferdous A (2014) Fli1 acts downstream of Etv2 to govern cell survival and vascular homeostasis via positive autoregulation. *Circ Res* 114: 1690 – 1699
23. Dejana E, Taddei A, Randi AM (2007) Foxs and Ets in the transcriptional regulation of endothelial cell differentiation and angiogenesis. *Biochim Biophys Acta* 1775: 298 – 312
24. Lee D, Park C, Lee H, Lugus JJ, Kim SH, Arentson E, Chung YS, Gomez G, Kyba M, Lin S *et al* (2008) ER71 acts downstream of BMP, Notch, and Wnt signaling in blood and vessel progenitor specification. *Cell Stem Cell* 2: 497 – 507
25. Ferdous A, Caprioli A, Iacovino M, Martin CM, Morris J, Richardson JA, Latif S, Hammer RE, Harvey RP, Olson EN *et al* (2009) Nk2–5 transactivates the Ets-related protein 71 gene and specifies an endothelial/endocardial fate in the developing embryo. *Proc Natl Acad Sci USA* 106: 814 – 819
26. Kataoka H, Hayashi M, Nakagawa R, Tanaka Y, Izumi N, Nishikawa S, Jakt ML, Tarui H (2011) Etv2/ER71 induces vascular mesoderm from Flk1+PDGFRalpha+ primitive mesoderm. *Blood* 118: 6975 – 6986
27. Liu F, Kang I, Park C, Chang LW, Wang W, Lee D, Lim DS, Vittet D, Nerbonne JM, Choi K (2012) ER71 specifies Flk-1+ hemangiogenic mesoderm by inhibiting cardiac mesoderm and Wnt signaling. *Blood* 119: 3295 – 3305
28. Waterston RH, Lindblad-Toh K, Birney E, Rogers J, Abril JF, Agarwal P, Agarwala R, Ainscough R, Alexandersson M, An P *et al* (2002) Initial sequencing and comparative analysis of the mouse genome. *Nature* 420: 520 – 562
29. Zhang Y, Liu T, Meyer CA, Eeckhoute J, Johnson DS, Bernstein BE, Nusbaum C, Myers RM, Brown M, Li W *et al* (2008) Model-based analysis of ChIP-Seq (MACS). *Genome Biol* 9: R137
30. Wilson NK, Foster SD, Wang X, Knezevic K, Schutte J, Kaimakis P, Chilarska PM, Kinston S, Ouwehand WH, Dzierzak E *et al* (2010) Combinatorial transcriptional control in blood stem/progenitor cells: genome-wide analysis of ten major transcriptional regulators. *Cell Stem Cell* 7: 532 – 544
31. McLean CY, Bristor D, Hiller M, Clarke SL, Schaar BT, Lowe CB, Wenger AM, Bejerano G (2010) GREAT improves functional interpretation of cis-regulatory regions. *Nat Biotechnol* 28: 495 – 501
32. Blanchette M, Kent WJ, Riemer C, Elnitski L, Smit AF, Roskin KM, Baertsch R, Rosenbloom K, Clawson H, Green ED *et al* (2004) Aligning multiple genomic sequences with the threaded blockset aligner. *Genome Res* 14: 708 – 715
33. Stadler MB, Murr R, Burger L, Ivanek R, Lienert F, Scholer A, van Nimwegen E, Wirbelauer C, Oakeley EJ, Gaidatzis D *et al* (2011) DNA-binding factors

 © 2015 The Authors

shape the mouse methylome at distal regulatory regions. *Nature* 480: 490 – 495

34. Hon GC, Rajagopal N, Shen Y, McCleary DF, Yue F, Dang MD, Ren B (2013) Epigenetic memory at embryonic enhancers identified in DNA methylation maps from adult mouse tissues. *Nat Genet* 45: 1198 – 1206
35. Wareing S, Mazan A, Pearson S, Gottgens B, Lacaud G, Kouskoff V (2012) The Flk1-Cre-mediated deletion of ETV2 defines its narrow temporal requirement during embryonic hematopoietic development. *Stem Cells* 30: 1521 – 1531
36. Pimanda JE, Ottersbach K, Knezevic K, Kinston S, Chan WY, Wilson NK, Landry JR, Wood AD, Kolb-Kokocinski A, Green AR *et al* (2007) Gata2, Fli1, and Scl form a recursively wired gene-regulatory circuit during early hematopoietic development. *Proc Natl Acad Sci USA* 104: 17692 – 17697
37. Lugus JJ, Chung YS, Mills JC, Kim SI, Grass J, Kyba M, Doherty JM, Bresnick EH, Choi K (2007) GATA2 functions at multiple steps in hemangioblast development and differentiation. *Development* 134: 393 – 405
38. Ismailoglu I, Yeamans G, Daley GQ, Perlingeiro RC, Kyba M (2008) Mesodermal patterning activity of SCL. *Exp Hematol* 36: 1593 – 1603
39. Liu F, Bhang SH, Arentson E, Sawada A, Kim CK, Kang I, Yu J, Sakurai N, Kim SH, Yoo JJ *et al* (2013) Enhanced hemangioblast generation and improved vascular repair and regeneration from embryonic stem cells by defined transcription factors. *Stem Cell Rep* 1: 166 – 182
40. Shi X, Richard J, Zirbes KM, Gong W, Lin G, Kyba M, Thomson JA, Koyano-Nakagawa N, Garry DJ (2014) Cooperative interaction of Etv2 and Gata2 regulates the development of endothelial and hematopoietic lineages. *Dev Biol* 389: 208 – 218
41. Takase H, Matsumoto K, Yamadera R, Kubota Y, Otsu A, Suzuki R, Ishitobi H, Mochizuki H, Kojima T, Takano S *et al* (2012) Genome-wide identification of endothelial cell-enriched genes in the mouse embryo. *Blood* 120: 914 – 923
42. Ema M, Takahashi S, Rossant J (2006) Deletion of the selection cassette, but not cis-acting elements, in targeted Flk1-lacZ allele reveals Flk1 expression in multipotent mesodermal progenitors. *Blood* 107: 111 – 117
43. Rasmussen TL, Shi X, Wallis A, Kweon J, Zirbes KM, Koyano-Nakagawa N, Garry DJ (2012) VEGF/Flk1 signaling cascade transactivates Etv2 gene expression. *PLoS ONE* 7: e50103
44. Kataoka H, Hayashi M, Kobayashi K, Ding G, Tanaka Y, Nishikawa S (2013) Region-specific Etv2 ablation revealed the critical origin of hemogenic capacity from Hox6-positive caudal-lateral primitive mesoderm. *Exp Hematol* 41: 567 – 581 e569
45. Zhang B, Zhou Y, Lin N, Lowdon RF, Hong C, Nagarajan RP, Cheng JB, Li D, Stevens M, Lee HJ *et al* (2013) Functional DNA methylation differences between tissues, cell types, and across individuals discovered using the M&M algorithm. *Genome Res* 23: 1522 – 1540
46. Grass JA, Jing H, Kim SI, Martowicz ML, Pal S, Blobel GA, Bresnick EH (2006) Distinct functions of dispersed GATA factor complexes at an endogenous gene locus. *Mol Cell Biol* 26: 7056 – 7067
47. Bresnick EH, Lee HY, Fujiwara T, Johnson KD, Keles S (2010) GATA switches as developmental drivers. *J Biol Chem* 285: 31087 – 31093
48. Kim JY, Lee RH, Kim TM, Kim DW, Jeon YJ, Huh SH, Oh SY, Kyba M, Kataoka H, Choi K *et al* (2014) OVOL2 is a critical regulator of ER71/ETV2 in generating FLK1+, hematopoietic, and endothelial cells from embryonic stem cells. *Blood* 124: 2948 – 2952
49. Hayashi M, Pluchinotta M, Momiyama A, Tanaka Y, Nishikawa S, Kataoka H (2012) Endothelialization and altered hematopoiesis by persistent Etv2 expression in mice. *Exp Hematol* 40: 738 – 750 e711
50. Morita R, Suzuki M, Kasahara H, Shimizu N, Shichita T, Sekiya T, Kimura A, Sasaki K, Yasukawa H, Yoshimura A *et al* (2015) ETS transcription factor ETV2 directly converts human fibroblasts into functional endothelial cells. *Proc Natl Acad Sci USA* 112: 160 – 165
51. Ginsberg M, James D, Ding BS, Nolan D, Geng F, Butler JM, Schachterle W, Pulijaal VR, Mathew S, Chasen ST *et al* (2012) Efficient direct reprogramming of mature amniotic cells into endothelial cells by ETS factors and TGFbeta suppression. *Cell* 151: 559 – 575
52. Motoike T, Markham DW, Rossant J, Sato TN (2003) Evidence for novel fate of Flk1+ progenitor: contribution to muscle lineage. *Genesis* 35: 153 – 159
53. Lee D, Kim T, Lim DS (2011) The Er71 is an important regulator of hematopoietic stem cells in adult mice. *Stem Cells* 29: 539 – 548
54. de Felipe P (2002) Polycistronic viral vectors. *Curr Gene Ther* 2: 355 – 378
55. Li H, Durbin R (2009) Fast and accurate short read alignment with Burrows-Wheeler transform. *Bioinformatics* 25: 1754 – 1760
56. Li D, Zhang B, Xing X, Wang T (2015) Combining MeDIP-seq and MRE-seq to investigate genome-wide CpG methylation. *Methods* 72: 29 – 40
57. Heinz S, Benner C, Spann N, Bertolino E, Lin YC, Laslo P, Cheng JX, Murre C, Singh H, Glass CK (2010) Simple combinations of lineage-determining transcription factors prime cis-regulatory elements required for macrophage and B cell identities. *Mol Cell* 38: 576 – 589
58. Lockstone HE (2011) Exon array data analysis using Affymetrix power tools and R statistical software. *Brief Bioinform* 12: 634 – 644

© 2015 The Authors